from zero to infinity. Thus, the change in the third moment is always less than $\langle\Delta E_{\pm}^3\rangle_{RS}$. An accurate measurement of $\langle\Delta E_{\pm}^3\rangle$ would allow a determination of x and thus the first quantitative determination of the contribution to the broadening by noncubic lattice vibrations. We have made preliminary measurements of the circular dichroism of the F center in KCl which indicate that $\langle\Delta E_{\pm}^3\rangle$ is significantly less than $\langle\Delta E_{\pm}^3\rangle_{RS}$. Similar observations have been communicated to us by Margerie and Romestain. These observations prove that the noncubic lattice vibrations are quite important.

In the same manner, we can analyze the stress experiments on the F center. We find the change in the third moment for a pressure is

$$\langle\Delta E_\eta^3\rangle=3\langle\Delta E_\eta\rangle\langle E^2\rangle, \quad \text{(A27)}$$

for a stress in the 100 direction is

$$(\langle\Delta E_{II}^3\rangle-\langle\Delta E_\perp^3\rangle)=3(\langle\Delta E_{II}\rangle-\langle\Delta E_\perp\rangle)\times(\langle E^2\rangle_1+\langle E^2\rangle_3+\tfrac{1}{2}\langle E^2\rangle_5), \quad \text{(A28)}$$

and for a stress in the 110 direction is

$$(\langle\Delta E_{II}^3\rangle-\langle\Delta E_\perp^3\rangle)=3(\langle\Delta E_{II}\rangle-\langle\Delta E_\perp\rangle)\times(\langle E^2\rangle_1+\tfrac{1}{2}\langle E^2\rangle_3+\tfrac{5}{6}\langle E^2\rangle_5). \quad \text{(A29)}$$

The line shape will thus appear to shift rigidly upon the application of a pressure. The line shape will not shift rigidly when an axial stress is applied and measurements of the change in the third moment in this case will yield $\langle E^2\rangle_3$ and $\langle E^2\rangle_5$.

If the spin-orbit splitting Δ becomes a large fraction of the linewidth, we must keep higher order terms in Δ in computing $\langle E^2\rangle$ and $\langle\Delta E_\eta^3\rangle$. Keeping the first term in Eq. (48), we find

$$\langle E^2\rangle=\langle E^2\rangle_C+\langle E^2\rangle_{NC}+2(\Delta/3)^2. \quad \text{(A30)}$$

Similarly, if we keep the last two terms in Eq. (54), we find in the magnetic case that

$$\langle\Delta E_{\pm}^3\rangle=3\langle\Delta E_{\pm}\rangle[\langle E^2\rangle_C+\tfrac{1}{2}(\langle E^2\rangle_{NC}+2(\Delta/3)^2)]. \quad \text{(A31)}$$

Using these equations, we have evaluated $\langle E^2\rangle_C$ and $\langle E^2\rangle_{NC}$ for CsBr and CsCl as discussed in Sec. VI.B.

PHYSICAL REVIEW VOLUME 137, NUMBER 2A 18 JANUARY 1965

Effect of Uniaxial Stress on the Excitation Spectra of Donors in Silicon*

R. L. AGGARWAL AND A. K. RAMDAS
Department of Physics, Purdue University, Lafayette, Indiana
(Received 31 August 1964)

The excitation spectra of neutral shallow group V donors in silicon, viz., phosphorus, antimony, and arsenic, have been measured with crystals subjected to compression, **F**, along the [100], [110], or [111] direction. Each excitation line is observed to undergo a splitting into two components for **F** ∥ [100] or **F**∥ [110], the spacing between the components being the same for all the lines. The spectra were measured with polarized light, the direction of polarization being either parallel or perpendicular to the compressive force. The split components of the excitation lines exhibit pronounced polarization. The splittings can be ascribed to the splitting of the excited p states arising from the energy shifts of the conduction-band minima in uniaxially stressed silicon. The polarization features have been interpreted on the basis of the new site symmetry of the substitutional donor atom in the stressed crystal. The absence of splittings for **F** ∥ [111] follows from the preservation of the energy equivalence of the six valleys even under stress.

I. INTRODUCTION

A SEMICONDUCTOR like silicon or germanium which has a multivalley conduction band exhibits many interesting effects when subjected to a uniaxial stress. Piezoresistance measurements carried out by Smith,[1] cyclotron resonance measurements on strained crystals of silicon and germanium reported by Rose-Innes,[2] and observations of photoelastic effects made by Schmidt-Tiedemann[3] are some examples of phenomena occurring on the application of uniaxial stress. These effects have been shown to arise from the shifts in energy of the various conduction band minima or valleys with respect to one another. The theoretical interpretations of these phenomena are based on the work of Herring,[5] and Herring and Vogt[6] which make use of the deformation potential theory. The donor states, described in the effective mass approximation, are intimately related to the nature of the conduction band and hence one might expect interesting strain effects associated with them. Price[7] and Kohn[8] have considered

* Work supported in part by the Advanced Research Projects Agency and the U. S. Army Research Office-Durham.

[1] C. S. Smith, Phys. Rev. **94**, 42 (1954).

[2] A. C. Rose-Innes, Proc. Phys. Soc. (London) **72**, 514 (1958).

[3] K. J. Schmidt-Tiedemann, *Proceedings of the International Conference on the Physics of Semiconductors, Exeter 1962* (The Institute of Physics and the Physical Society, London, 1962), p. 191.

[4] R. W. Keyes, *Solid State Physics*, edited by F. Seitz and D. Turnbull (Academic Press Inc., New York, 1960), Vol. 11, p. 149.

[5] C. Herring, Bell System Tech. J. **34**, 237 (1955).

[6] C. Herring and E. Vogt, Phys. Rev. **101**, 944 (1956).

[7] P. J. Price, Phys. Rev. **104**, 1223 (1956).

[8] W. Kohn, *Solid State Physics*, edited by F. Seitz and D. Turnbull (Academic Press Inc., New York, 1957), Vol. 5, p. 257.

this problem theoretically. Weinreich and White[9] have reported experimental observations on the effect of uniaxial stress on the excitation spectra of arsenic and phosphorus impurities in germanium. Their experiments were directed towards the determination of the valley-orbit splittings of the ground state of shallow donors in germanium and were performed without the use of polarized radiation. The present authors have presented brief reports[10,11] on the effect of uniaxial stress on the excitation spectra of group V donors in silicon observed with polarized light. The purpose of the present paper is to give a detailed account of this work.

We have observed splittings of excitation lines of the donor electron when the silicon crystal is subjected to a uniaxial compression. The mean positions of the split components are shifted from the positions of lines for zero stress. The most striking result of the present investigation is the pronounced polarization effects exhibited by the lines split by the applied stress. All these features show a marked dependence on the crystallographic orientation of the stress. The experimental results are presented in Sec. III. The interpretation of the data given in Sec. V, is based on the theoretical background developed in Sec. IV. The interpretation makes use of the deformation potential theory and the symmetry of the donor site, both these aspects being taken into account via the effective mass theory of Kohn and Luttinger.[12] The polarization features have been deduced from the symmetry classification of the split donor levels using the group theoretical technique described by Ramdas, Lee, and Fisher.[13]

II. EXPERIMENTAL PROCEDURE

Single crystals of silicon doped with phosphorus, antimony or arsenic impurities in the range $10^{14}-10^{16}/\text{cm}^3$ were used in the present measurements. The samples were cut in the desired crystallographic directions, after orienting them either by x-ray or the optical method described by Hancock and Edelman.[14] In the present studies uniaxial compression was applied parallel to the [100], [110], or [111] direction.

A double-pass Perkin-Elmer grating monochromator, equipped with Bausch and Lomb plane reflection gratings and appropriate filtering systems, was used for the measurements. The radiation was polarized by passing it through a set of twenty-four polyethylene films, mounted at the Brewster's angle.[15] An optical cryostat[16] was used to make the transmission measurements at liquid-helium temperatures, using a Reeder thermocouple with a diamond window as the detector.

The uniaxial compression was produced by following the technique described by Rose-Innes.[2] In this technique the silicon sample is constrained in a copper jig, and the whole assembly attached to the copper tail of the cryostat. During the cooling process from room temperature to liquid-helium temperature, copper contracts more than silicon. This differential contraction is uniaxial in view of the geometry of the copper frame and the silicon sample. Using the relative change in length with temperature reported in the literature for silicon[17] and copper,[18] one expects strains of the order of 10^{-3}, assuming the entire differential contraction were effective. This corresponds to a stress $\sim 10^9$ dyn/cm^2 in the [100] direction. In the actual experimental procedure grease is applied to the two ends of the sample which forms a solid bond between the copper frame and the sample when it freezes during the cooling from room temperature. The formation of the bond thus depends on the freezing point of the grease employed. A certain amount of slippage of the sample is to be expected before the freezing occurs. Thus the actual strain is expected to be less than what would have been produced if the entire differential contraction were effective. In fact it is possible to produce different strains by employing greases of different specifications. In the present work the actual strain was not directly determined.

III. EXPERIMENTAL RESULTS

In Figs. 1–5 are presented the excitation spectra of phosphorus impurity in silicon for uniaxial compression, $\mathbf{F}$, along [100], [110]or [111] and for electric vector $\mathbf{E}$, either parallel or perpendicular to $\mathbf{F}$. In Fig. 1 is also given the spectrum for $\mathbf{F}=0$, whereas in the other figures the positions of the excitation lines for zero stress are indicated by dotted vertical lines.

The following features are noticed in Fig. 1, for $\mathbf{F}\|[100]$:

(a) The line corresponding to $1s(A_1)\rightarrow 2p_0$ splits into two components, one on either side of the zero stress position.

(b) The split components show pronounced polarization, i.e., the low-energy component, $2p_0(-)$, appears only for $\mathbf{E}\|\mathbf{F}$ whereas the high-energy component, $2p_0(+)$, appears only for $\mathbf{E}\perp\mathbf{F}$.

(c) The mean position of the two components is shifted to the low-energy side of the zero-stress position.

[9] G. Weinreich and H. G. White, Bull. Am. Phys. Soc. **5**, 60 (1960); and G. Weinreich, *Proceedings of the International Conference on Semiconductor Physics, Prague 1960* (Czechoslovak Academy of Sciences, Prague, 1961), p. 360.

[10] R. L. Aggarwal and A. K. Ramdas, Bull. Am. Phys. Soc. **9**, 278 (1964).

[11] R. L. Aggarwal and A. K. Ramdas, in *Proceedings of the International Conference on the Physics of Semiconductors, Paris, 1964* (to be published).

[12] W. Kohn and J. M. Luttinger, Phys. Rev. **98**, 915 (1955).

[13] A. K. Ramdas, P. M. Lee, and P. Fisher, Phys. Letters **7**, 99 (1963).

[14] R. D. Hancock and S. Edelman, Rev. Sci. Instr. **27**, 1082 (1956).

[15] A. Mitsuishi, Y. Yamada, S. Fujita, and H. Yoshinaga, J. Opt. Soc. Am. **50**, 433 (1960).

[16] P. Fisher, W. H. Haak, E. J. Johnson, and A. K. Ramdas, *Proceedings of the Eighth Symposium on the Art of Glassblowing* (The American Scientific Glassblowers Society, Wilmington, Delaware, 1963), p. 136.

[17] D. F. Gibbons, Phys. Rev. **112**, 136 (1958).

[18] D. Bijl and H. Pullan, Physica **21**, 285 (1955).

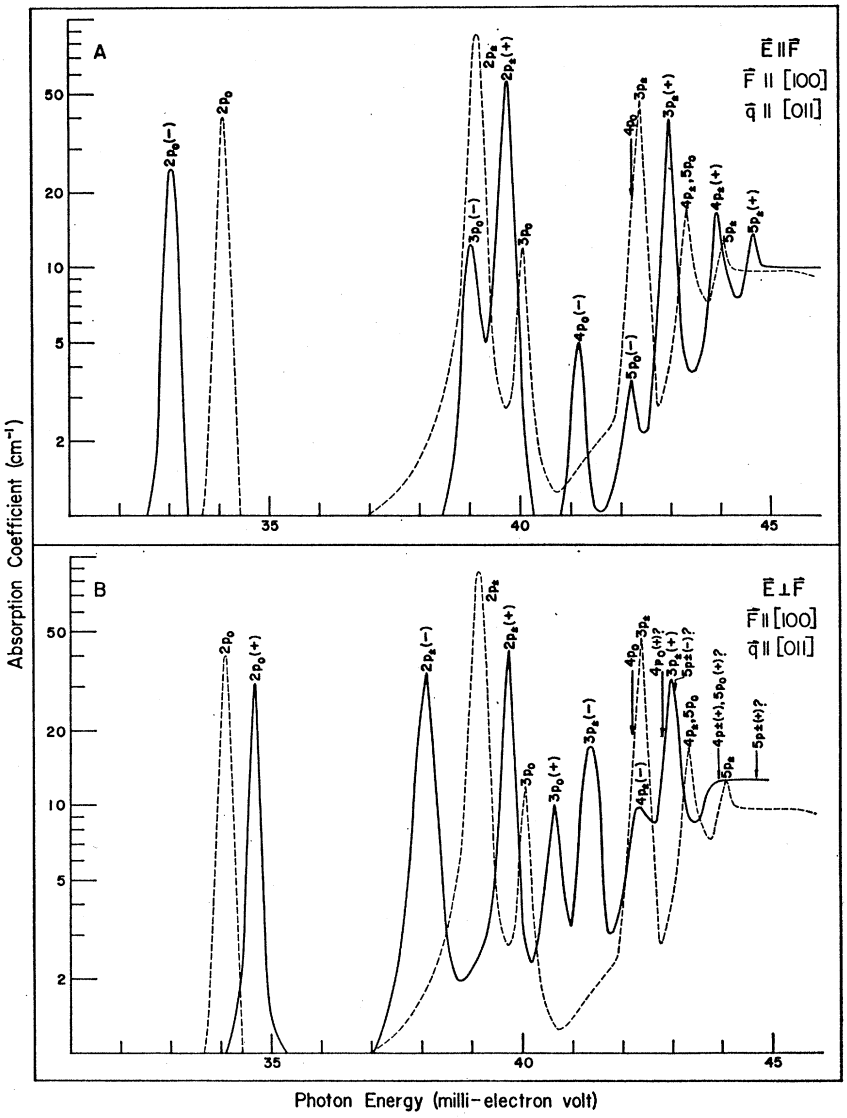

FIG. 1. Excitation spectrum of phosphorus in silicon [ρ(300°K) $=0.9\ \Omega$ cm] under uniaxial compression, **F**, along [100]. A—The electric vector **E**$\|$**F**. B—**E**$\perp$**F**. The dotted curve is for **F**$=0$.

(d) Denoting the spacings [$2p_0-2p_0(-)$] and [$2p_0(+)-2p_0$] by α and β, respectively, one finds components at positions $-\alpha$ and $+\beta$ from the zero-stress positions of the transitions to $2p_\pm$, $3p_0$, and $3p_\pm$ states. (The information regarding the components corresponding to $4p_0$, $4p_\pm$, $5p_0$, and $5p_\pm$ for **E**$\perp$**F** is incomplete as not all the expected components could be observed, presumably because of insufficient resolution.)

(e) The polarization characteristics of all the low-energy components of lines labeled by $m=0$, i.e., $2p_0(-)$, $3p_0(-)$, etc., are identical. The same is true of all the high-energy components, viz., $2p_0(+)$, $3p_0(+)$, etc. For example, the component $3p_0(+)$ appears for **E**$\perp$**F** and $3p_0(-)$ for **E**$\|$**F**.

(f) The polarization features of all the low-energy components with $m=\pm1$ are identical, i.e., $2p_\pm(-)$, $3p_\pm(-)$, etc., exhibit the same type of polarization. They all appear only for **E**$\perp$**F**. All the high-energy components $2p_\pm(+)$, $3p_\pm(+)$, etc., appear for both **E**$\|$**F** and **E**$\perp$**F**. Thus the lines characterized by $m=\pm1$ show markedly different stress induced polarization effects compared to those manifested by the $m=0$ lines.

Figures 2–4 depict the results obtained when **F** is applied along [110]. They, however, refer to different directions of light propagation. Once again it is noticed that all the excitation lines show two components, one on either side of the zero-stress position. In each figure the low-energy components are displaced by the same energy from the zero-stress position and so also the high-energy components. For this orientation the mean position of the split components lies on the high-energy side of the zero-stress position, in contrast to the **F**$\|$[100] case. Again, all the corresponding components of the excitation lines with $m=0$ show identical polariza-

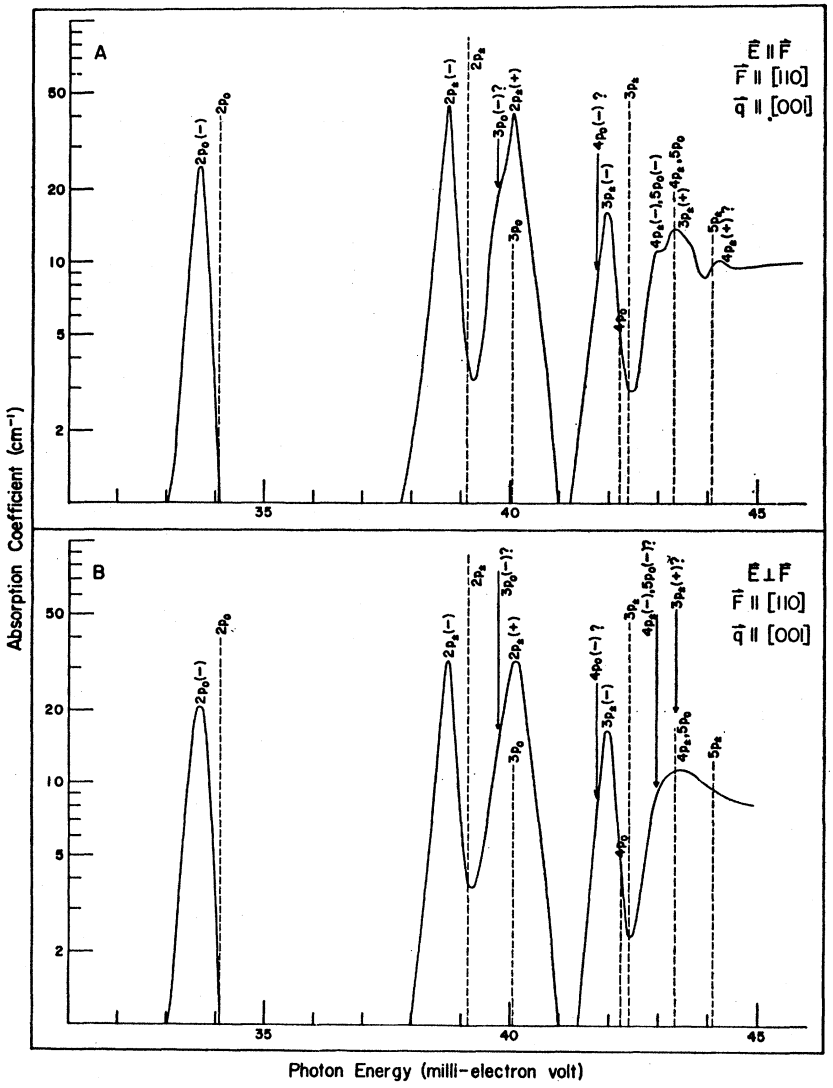

FIG. 2. Excitation spectrum of phosphorus in silicon [$\rho(300°K) = 0.9\ \Omega$ cm] with compression along [110] and the direction of light propagation, **q**, along [001]. A—$\mathbf{E} \| \mathbf{F}$ and B—$\mathbf{E} \perp \mathbf{F}$. The dotted vertical lines indicate the positions of the excitation lines for zero stress.

tion features. The same remark holds good for the lines characterized by $m = \pm 1$. However, for this direction of **F**, there is an additional important factor, viz., the direction of light propagation vector, **q**. In the first place, the spectrum is the same for $\mathbf{E} \| \mathbf{F}$ irrespective of **q**. For $\mathbf{E} \perp \mathbf{F}$, however, very striking differences are found for $\mathbf{q} \| [001]$, $[1\bar{1}0]$, and $[11\bar{2}]$, respectively. For $\mathbf{q} \| [010]$ (see Fig. 2), the high-energy components for $m=0$ lines, i.e., $2p_0(+)$, $3p_0(+)$, etc., are completely absent for both $\mathbf{E} \| \mathbf{F}$ and $\mathbf{E} \perp \mathbf{F}$. However, for $\mathbf{q} \| [1\bar{1}0]$ (see Fig. 3), these high-energy components are observed for $\mathbf{E} \perp \mathbf{F}$. The $2p_0(-)$ line is observed for both $\mathbf{E} \| \mathbf{F}$ and $\mathbf{E} \perp \mathbf{F}$ in $\mathbf{q} \| [001]$ orientation and only for $\mathbf{E} \| \mathbf{F}$ for $\mathbf{q} \| [1\bar{1}0]$. The $\mathbf{q} \| [11\bar{2}]$ represents a direction where effects of $\mathbf{q} \| [001]$ and $[1\bar{1}0]$ are superimposed, i.e., the $2p_0(-)$ line is observed for both $\mathbf{E} \| \mathbf{F}$ and $\mathbf{E} \perp \mathbf{F}$ on the one hand, and, on the other hand, $2p_0(+)$ line is observed for $\mathbf{E} \perp \mathbf{F}$ (see Fig. 4). For the lines with $m = \pm 1$, the low-energy components, $2p_\pm(-)$, $3p_\pm(-)$, etc., are observed for both $\mathbf{E} \| \mathbf{F}$ and $\mathbf{E} \perp \mathbf{F}$ for all three directions of propagation. The high-energy components, $2p_\pm(+)$, $3p_\pm(+)$, etc., however, show the following behavior: with $\mathbf{q} \| [001]$, they are observed for both $\mathbf{E} \| \mathbf{F}$ and $\mathbf{E} \perp \mathbf{F}$ and with $\mathbf{q} \| [1\bar{1}0]$, they are absent for $\mathbf{E} \perp \mathbf{F}$. The effects for $\mathbf{q} \| [11\bar{2}]$ are a superposition of the effects for $\mathbf{q} \| [001]$ and $\mathbf{q} \| [1\bar{1}0]$. As can be seen from Figs. 2–4, it has not been possible to observe in a given experiment all the components for the excited states above $3p_\pm$. The splitting and the polarization features have to be such as to favor a clear resolution of the components for a given **F**, **E**, and **q**.

As can be seen from Fig. 5, splittings and polarization effects are negligibly small for $\mathbf{F} \| [111]$.

Observations with antimony- or arsenic-doped silicon give the same results as described above.

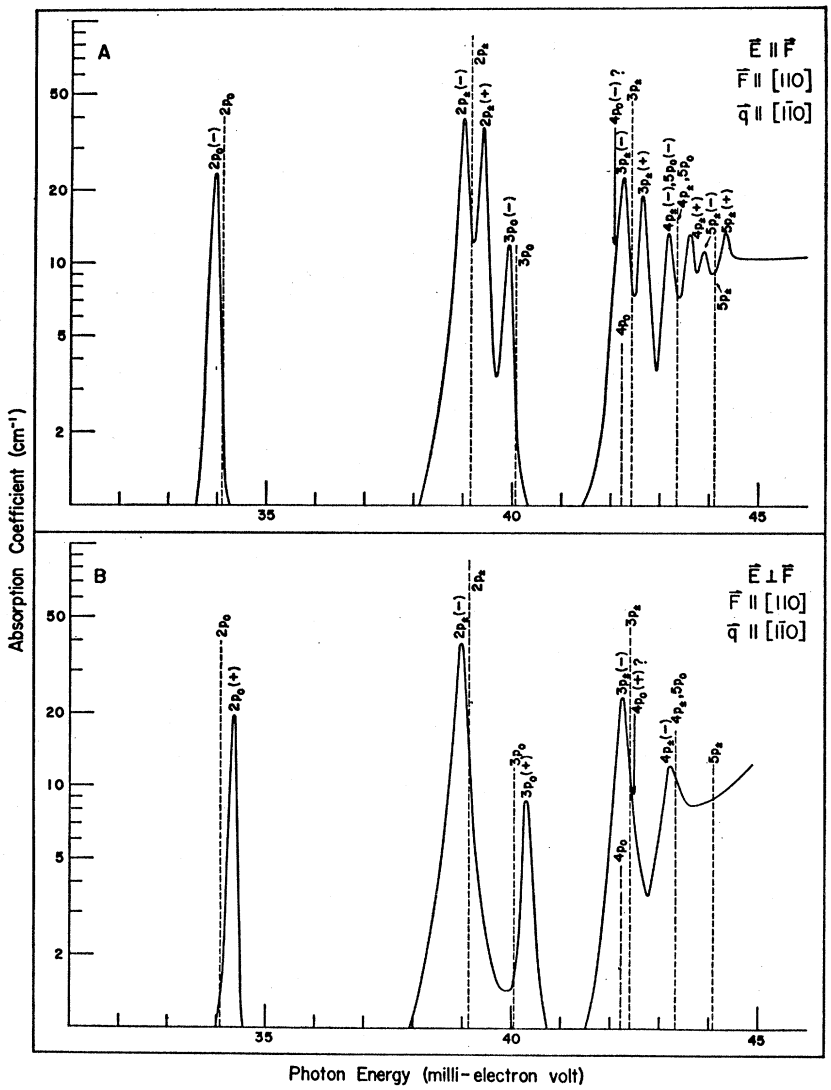

FIG. 3. Excitation spectrum of phosphorus in silicon [$\rho(300°K) = 0.9\ \Omega$ cm] with $\mathbf{F} \parallel [110]$ and $\mathbf{q} \parallel [1\bar{1}0]$. A—$\mathbf{E} \parallel \mathbf{F}$ and B—$\mathbf{E} \perp \mathbf{F}$.

IV. INTERPRETATION OF RESULTS: THEORETICAL CONSIDERATIONS

A. Excitation Spectrum for Zero Stress

It is useful to summarize here the important theoretical results concerning the excitation spectra of group V donors in silicon. The energy level scheme for the donor electron bound to the donor impurity has been calculated for a multivalley semiconductor by Kohn and Luttinger[8,12] in the effective mass approximation. This theory leads to donor wave functions which are linear combinations of the following type:

$$\psi(\mathbf{r}) = \sum_{j=1}^{N} \alpha^{(j)} F^{(j)}(\mathbf{r}) \Phi^{(j)}(\mathbf{r}), \qquad (1)$$

where $\Phi^{(j)}(\mathbf{r})$ are Bloch functions at the jth minimum, $F^{(j)}(\mathbf{r})$ are effective mass envelope functions, $\alpha^{(j)}$ are numerical coefficients which describe the relative contribution from each valley, $N=6$ for the case of silicon, the valleys being along $\langle 100 \rangle$.

Figure 6 shows the enregy-level scheme for s-like and p-like states. As a result of the axial symmetry for the Schrödinger equation satisfied by the envleope functions, the $(2l+1)$ degeneracy of a hydrogenic level is lifted and levels corresponding to $m=0, \pm 1, \pm 2$, are separated energetically. The irreducible representations of the tetrahedral point group T_d for which the wave functions of a given state form a basis, are shown next to the level. In the effective mass approximation foı silicon, each level is sixfold degenerate owing to the six energetically equivalent conduction-band minima. Experimentally, the spacings between the excitation lines for various group V impurities are the same though the actual positions vary from impurity to impurity. (See Table I.) This is taken as evidence of the success of the effective mass approximation for the excited p states

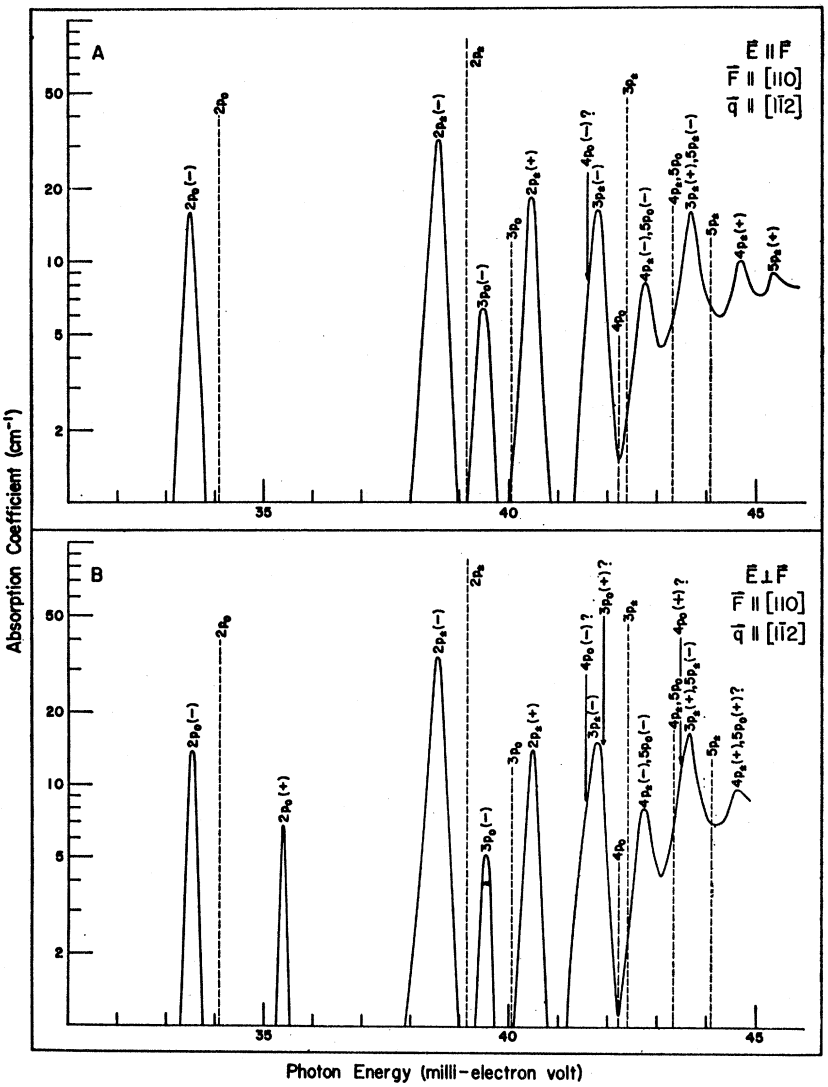

FIG. 4. Excitation spectrum of phosphorus in silicon [$\rho(300°K) = 0.9\ \Omega$ cm] with $\mathbf{F} \| [110]$ and $\mathbf{q} \| [1\bar{1}2]$. A—$\mathbf{E} \| \mathbf{F}$ and B—$\mathbf{E} \perp \mathbf{F}$.

and its breakdown for the $1s$ ground state. The latter has its origin in the so-called "valley-orbit" splitting or "chemical" splitting for the $1s$ ground state. The effective mass approximation breaks down in the vicinity of the impurity, this being most significant for the s-like states. The sixfold degenerate $1s$ state splits into $1s(A_1)$, $1s(E)$, and $1s(T_1)$ states with degeneracies 1, 2, and 3, respectively. Again, the departure from the "effective mass" position is expected[8] to be most drastic for the $1s(A_1)$ state while the $1s(E)$ and $1s(T_1)$ states are still expected to be described satisfactorily in the effective mass approximation. Recent experimental results reported by one of us[19] show that $1s(A_1) - 1s(T_1) = D = 11.85$, 9.94, and 21.15 meV for phosphorus, antimony and arsenic, respectively. The $1s(T_1)$ state lies below $1s(E)$, their separation, d, being 1.35, 2.50, and 1.42 meV for phosphorus, antimony and arsenic, respectively.

[19] R. L. Aggarwal, Solid State Commun. 2, 163 (1964).

In the present work, the sample being at liquid helium temperatures, the excitation lines arise from the lowest $1s$ level, which is $1s(A_1)$ for zero stress.

B. Effect of Uniaxial Stress on Donor Levels: Energy Considerations

When a uniaxial stress is applied to silicon, the conduction-band minima shift in energy with respect to one another. Following Herring's deformation potential analysis[5] one can write the shift in energy of the jth minimum as

$$\Delta E^{(j)} = [\Xi_d \delta_{\alpha\beta} + \Xi_u K_\alpha^{(j)} K_\beta^{(j)}] u_{\alpha\beta}, \qquad (2)$$

where $K_\alpha^{(j)}$, $K_\beta^{(j)}$ are components of a unit vector pointing from the center of the Brillouin Zone towards the position in k space of the jth minimum. The subindex α or β designates a component along one of the cubic axes of the crystal. The deformation potentials

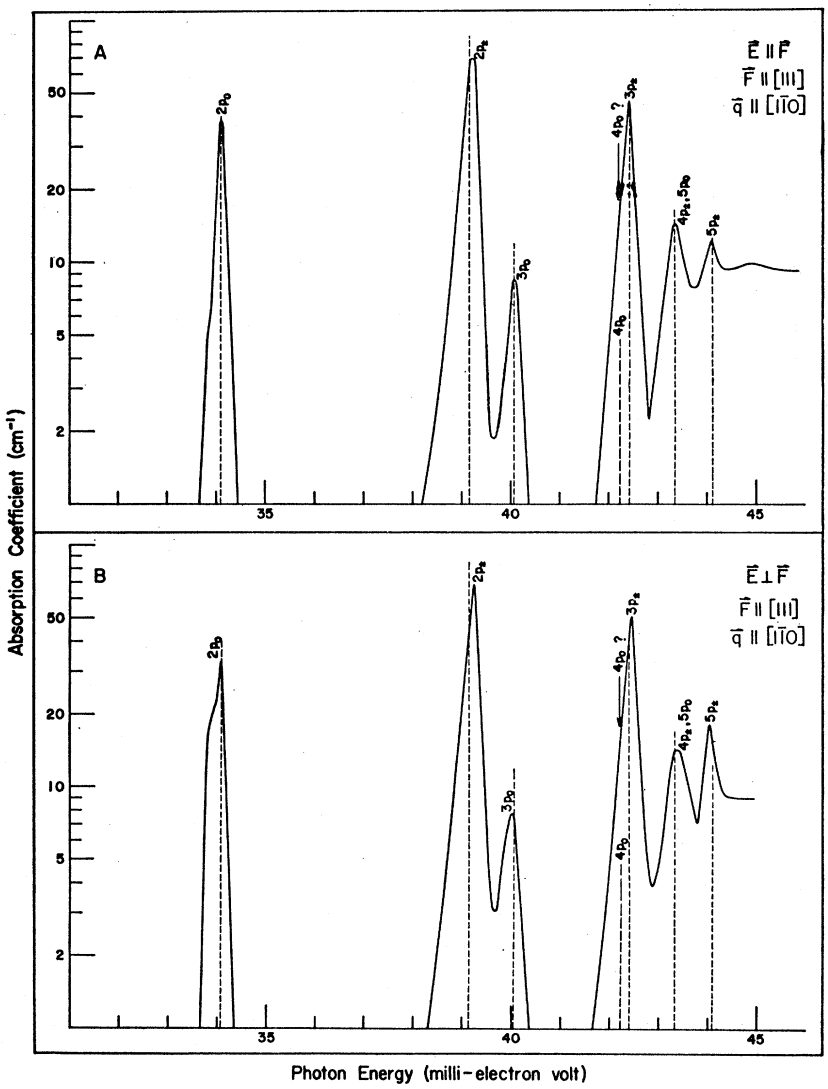

FIG. 5. Excitation spectrum of phosphorus in silicon [$\rho(300°K) = 0.9\ \Omega$ cm] with $\mathbf{F} \| [111]$. A—$\mathbf{E} \| \mathbf{F}$ and B—$\mathbf{E} \perp \mathbf{F}$.

Ξ_d and Ξ_u are defined as follows: Ξ_d is the valley shift due to a dilation in the two directions normal to the valley axis and Ξ_u is the shift due to a uniaxial shear compounded of a stretch along the valley axis and a contraction in the two normal directions and $u_{\alpha\beta}$ are the components of the strain tensor. In Eq. (2) a summation over α and β is implied. As has been shown by Price,[7] the excited p states, for which the valley-orbit splitting is negligible, split into as many components as there are energetically different valleys. In the effective mass approximation, each set of valleys with the same energy, will give rise to a particular component from among the several components into which a given donor-level splits under stress. The separation of this component from the zero-stress position of the donor level can be shown[7,20] to be equal to the shift of the corresponding valleys from their zero-stress energy. Thus, in this approximation all the excited p states will exhibit an identical energy-level scheme under strain both with respect to the number of components and the magnitude of their splittings. It has also been shown[20] that the $1s(A_1)$ state shifts under uniaxial stress and the linear combination of the wave functions corresponding to it undergoes a change in the coefficients $\alpha^{(j)}$ characterizing contributions from the various valleys. However, it still remains nondegenerate, and for the stresses employed, there is no level close to it to be significantly populated at the temperature of measurement. Corresponding to a particular zero-stress excitation line, one should thus expect as many components as there are energetically different valleys on the application of the stress, provided the selection rules allow them. From the spacings of the lines one can calculate the deformation potential constant, Ξ_u, using Eq. (2). The actual positions of the lines include the shift of the $1s(A_1)$ level and from the analysis of the spacings and

[20] D. K. Wilson and G. Feher, Phys. Rev. **124**, 1068 (1961).

the position one can deduce the valley-orbit splittings.[9] In the above analysis the changes in effective mass and/or dielectric constant are ignored as their effects are expected to be negligible for the stresses employed.[21]

C. Effect of Uniaxial Stress on Donor Levels: Symmetry Considerations

When a perturbing external field is applied to a crystal, the symmetry of the crystal is lowered since all the symmetry operations which it possessed for zero stress are no longer applicable. It is possible to find the new crystal symmetry under the application of the uniaxial stress by assuming that the crystal has symmetry elements common to the strain ellipsoid and the crystal before the application of the stress. Such a procedure has been developed by Peiser, Wachtman, and Dickson.[22] Once the new space group is deduced in this fashion, one can immediately discover the new site symmetry of the donor impurity.

As in the case of zero stress, the wave functions of the donor electron are linear combinations of wave functions labeled by the valley number. The wave functions of the donor electron form the basis of the irreducible representations of the site symmetry group, whereas the "valley" wave functions, i.e., the wave functions labeled according to a given valley, form a basis of the "valley" symmetry group. By "valley" symmetry group is meant the group consisting of symmetry elements of the site group which leave a given valley undisplaced; hence the "valley" group is a subgroup of the site group. From a knowledge of the irreducible representations for which the valley wave functions form a basis, one can generate the irreducible representations of the "site" group by the use of the Frobenius' reciprocity theorem.[13] It is clear that those valleys which are related by a symmetry element of the site group will have been identically affected by the perturbation and can be grouped into symmetry types. The representations of the site group

TABLE I. Spacings of excited donor states in silicon. Units are millielectron volts.

States	Theory[a]	P[b]	As	Sb[b]	Bi[d]
$2p_\pm-2p_0$	5.0±0.3	5.06	5.12[b]	5.06	4.94
$3p_0-2p_\pm$	0.2±0.7	0.93	0.86[b]	0.95	0.93
$3p_\pm-2p_\pm$	3.0±0.15	3.27	3.25[b]	3.34	3.31
$4p_0-2p_\pm$	···	3.11	2.6[c]	?	2.61
$4p_\pm-2p_\pm$	···	4.21	4.3[c]	4.33	4.35
$5p_0-2p_\pm$	···	4.21	4.3[c]	4.33	4.34
$5p_\pm-2p_\pm$	···	4.95	4.9[c]	?	5.26

[a] See Ref. 12.
[b] The experimental values are based on our measurements. The experimental error is ±0.05 units.
[c] J. W. Bichard and J. C. Giles, Can. J. Phys. 40, 1480 (1962).
[d] S. Zwerdling, K. J. Button, and B. Lax, Group Report M84-4 of the Lincoln Laboratory, Massachusetts Institute of Technology (unpublished). The spacings are calculated from the average zero field positions of the transitions.

[21] M. G. Holland and W. Paul, Phys. Rev. **128**, 30 (1962).
[22] H. S. Peiser, J. B. Wachtman, Jr., and R. W. Dickson, J. Res. Natl. Bur. Std. A, **67**, 395 (1963).

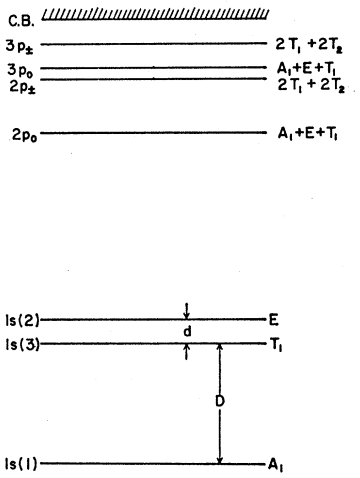

FIG. 6. Energy level scheme (not to scale) for s-like and p-like states of the donor electron in silicon. The letters next to a level indicate the representations of the site symmetry, T_d.

generated by different valley symmetry types will correspond to energetically different levels and, in fact, the grouping according to energy is deduced using Eq. (2). Thus the final energy level scheme can be labeled according to the valley symmetry type.[23] These deductions apply to the excited p-like states with no valley-orbit splitting.

As we have seen before, the lowest $1s(A_1)$ ground state in silicon continues to be nondegenerate. The reduction of the tetrahedral point group T_d into the new site symmetry group, shows that the wave function of the $1s(A_1)$ ground state forms the basis of the totally symmetric representation of the new site symmetry group.

In this manner the irreducible representations defined by the excited state wave functions as well as that defined by the ground-state wave function can be deduced when a uniaxial stress is applied. One can now apply the standard group theoretical procedure[24] to deduce the selection rules for dipole transitions from the totally symmetric ground state to the various excited p states. The polarization features follow then as a natural consequence of the selection rules.

Attention should be drawn here to some of the important consequences of the above symmetry arguments. Consider the symmetry classification of all the excited p states with the magnetic quantum number $m=0$. The irreducible representations originating from one set of energetically equivalent valleys are the same for all the principal quantum numbers, i.e., for the components of $2p_0$, $3p_0$, $4p_0$, etc., states separated by the same energy

[23] One can also deduce the representations of the component of a donor level arising from a set of energetically equivalent valleys in a somewhat different manner. This is done by first deducing the character of the reducible representation of the new site symmetry for which the wave functions labeled by energetically equivalent valleys form the basis and then effecting the decomposition into irreducible representations following the standard group theoretical procedure.
[24] See for example, L. D. Landau and E. M. Lifshitz, *Quantum Mechanics*, translated by J. B. Sykes and J. S. Bell (Pergamon Press Ltd., London, 1958), p. 343.

from their respective zero stress positions. Components originating from different sets of valleys are characterized, in general, by different sets of irreducible representations. Hence transitions to different components have their own characteristic polarization features. Similar remarks apply to levels characterized by $m=\pm 1$. More importantly, the $m=0$ levels, on the one hand, and $m=\pm 1$ levels on the other give rise to polarization features which are characteristic of them and distinguish them from one another.

V. DISCUSSION

Experimental observations as already described in Sec. III, show that all the excitation lines split into two lines for $\mathbf{F}\|[100]$ or $\mathbf{F}\|[110]$, the spacings between the components being the same for all the excitation lines. No significant splittings are observed for $\mathbf{F}\|[111]$. According to the arguments developed in the previous section, one expects as many components as there are energetically different valleys and the energy separation of an excited p-state component from its zero stress position is equal to the energy shift of the corresponding valleys from their original position. Using Eq. (2), the excitation lines are thus expected to split into two components for both $\mathbf{F}\|[100]$ and $\mathbf{F}\|[110]$ in agreement with observations. For $\mathbf{F}\|[111]$, all six valleys remain energetically equivalent and hence the absence of splittings is as expected.

The spacing between the high-energy component $E(+)$ and the low-energy component $E(-)$ turns out to be

$$E(+)-E(-)=-\tfrac{1}{2}\Xi_u s' \text{ for } \mathbf{F}\|[100], \quad (3)$$

and

$$E(+)-E(-)=-\tfrac{1}{4}\Xi_u s' \text{ for } \mathbf{F}\|[110] \quad (4)$$

where $s'=2(s_{11}-s_{12})T$, s_{11} and s_{12} being the elastic compliance constants and T being the applied compression. Thus, Eqs. (3) and (4) give a direct way of determining the deformation potential constant Ξ_u from the experimentally determined spacing, $E(+)-E(-)$, and s'.

It can be easily shown[20] that, for compression along [100], the four valleys normal to the compression have an energy $(\frac{1}{6})\Xi_u s'$ above and the two valleys along the compression $(\frac{1}{3})\Xi_u s'$ below the center of gravity of their energies under stress. Besides, the spacing between the center of gravity of an excited state and the $1s(A_1)$ level increases by an amount much smaller than the shifts of the individual components of the excited state from the center of gravity. The experimental fact that the mean position of the split lines lies toward the low-energy side of the zero-stress position thus follows as a consequence. A similar explanation can be given for $\mathbf{F}\|[110]$.

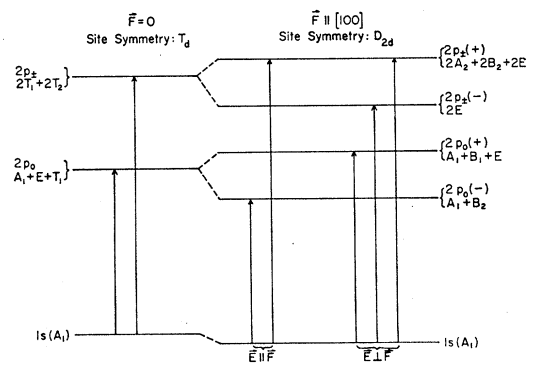

FIG. 7. Energy levels (not to scale) for $\mathbf{F}=0$ and $\mathbf{F}\|[100]$. The arrows indicate the allowed transitions. The letters next to a level denote the representations of the appropriate site symmetry.

Let us now consider the symmetry arguments to deduce the polarization features for compression along [100]. The following symmetry operations are no longer applicable to the site symmetry of the substitutional impurity: the fourfold rotation-reflection axes parallel to [010] and [001]; all the threefold axes along ⟨111⟩; the diagonal reflection planes $(1\bar{1}0)$, (110), (101), and $(\bar{1}01)$. Also, the twofold axis of rotation along [100] is not equivalent to those parallel to [010] and [001]. Under these conditions, the new site symmetry[25] is the tetragonal point group D_{2d} with the fourfold rotation-reflection axis along [100]. Table II shows the actual steps used in deducing the representations defined by wave functions labeled according to energetically equivalent valleys. Figure 7 shows the lowest $1s$ state $1s(A_1)$ and the excited p states for $\mathbf{F}\|[100]$ and $\mathbf{F}=0$. The new selection rules for dipole transitions under the application of stress, i.e., for the point group D_{2d}, can be deduced using the standard group theoretical procedure. The dipole transitions are polarized either parallel to the fourfold rotation-reflection axis [100] or perpendicular to it. For $\mathbf{E}\|\mathbf{F}$, only transitions to $2p_0(-)$ and $2p_\pm(+)$ from $1s(A_1)$ are allowed. Comparison with Fig. 1 shows that this is the case. For $\mathbf{E}\perp\mathbf{F}$, $1s(A_1)\rightarrow 2p_0(+)$, $1s(A_1)\rightarrow 2p_\pm(-)$, and $1s(A_1)\rightarrow 2p_\pm(+)$ transitions are allowed, a prediction confirmed by experiment as can be seen from Fig. 1. Since all the states labeled by $m=0$ generate the same representations, all the transitions to the high-energy components, i.e., to $2p_0(+)$, $3p_0(+)$, $4p_0(+)$, etc., will be observed for $\mathbf{E}\perp\mathbf{F}$ only, and all the transitions to $2p_0(-)$, $3p_0(-)$, $4p_0(-)$, etc., will be observed for $\mathbf{E}\|\mathbf{F}$ only. This is actually the case experimentally. Similarly, theory predicts and experimental observations confirm, that $1s(A_1)\rightarrow 2p_\pm(+)$, $3p_\pm(+)$ or $4p_\pm(+)$ should be observed for both $\mathbf{E}\|\mathbf{F}$ and $\mathbf{E}\perp\mathbf{F}$ whereas $1s(A_1)\rightarrow 2p_\pm(-)$, $3p_\pm(-)$, $4p_\pm(-)$, etc., should be observed for $\mathbf{E}\perp\mathbf{F}$ only. It is interesting to note here that the lines corresponding to levels higher than $3p_\pm$ were first identified for the case of bismuth donor by Zwerdling *et al.*[26] on the basis of the Zeeman effect studies of the excitation

[25] E. B. Wilson, Jr., J. C. Decius, and P. C. Cross, *Molecular Vibrations* (McGraw-Hill Book Company, Inc., New York, 1955), p. 328

[26] S. Zwerdling, K. J. Button, and B. Lax, Phys. Rev. **118**, 975 (1960).

TABLE II. Classification of p states of donors in silicon under uniaxial compression.

Direction of compression	Symmetry of impurity	Symmetry of valleys[a]	m	Γ ($C_{\infty v}$) $F=0$	Γ (valley) $F\neq 0$	Γ (impurity) $F\neq 0$	Level scheme $F=0$	Level scheme $F\neq 0$
[100]	D_{2d}	$C_2(3,4,5,6)$			A	A_1+B_1+E		$-A_1+B_1+E$
			0	A_1			A_1+E+T_1-	
		$C_{2v}(1,2)$			A_1	A_1+B_2		$-A_1+B_2$
		$C_2(3,4,5,6)$			$2B$	$2A_2+2B_2+2E$		$-2A_2+2B_2+2E$
			± 1	E_1			$2T_1+2T_2-$	
		$C_{2v}(1,2)$			B_1+B_2	$2E$		$-2E$
[110]	C_{2v}	$C_{2v}(5)(6)$			A_1	$2A_1$		$-2A_1$
			0	A_1			A_1+E+T_1-	
		$C_1(1,2,3,4)$			A	$A_1+A_2+B_1+B_2$		$-A_1+A_2+B_1+B_2$
		$C_{2v}(5)(6)$			B_1+B_2	$2(B_1+B_2)$		$-2(B_1+B_2)$
			± 1	E_1			$2T_1+2T_2-$	
		$C_1(1,2,3,4)$			$2A$	$2A_1+2A_2+2B_1+2B_2$		$-2A_1+2A_2+2B_1+2B_2$

[a] The numbers in parenthesis label the valleys and indicate to which subgroup a given valley belongs. The valleys are numbered as follows: 1—[100], 2—[$\bar{1}$00), 3—[010], 4—[0$\bar{1}$0], 5—[001], and 6—[00$\bar{1}$].

lines. They were not calculated by Kohn and Luttinger.[12] From the comparison of the spacing between, say, $3p_\pm$ and $4p_\pm$ in bismuth, similar higher lying levels have also been located for phosphorus, antimony, and arsenic. The stress effects reported here enable such assignments to be verified unambiguously. Also weak excitation lines, which lie so close to strong lines that it is experimentally difficult to resolve them, can be identified under stress. This is possible whenever the stress induced polarization features are different for the components of the two lines, and the magnitude of stress is optimum for the purpose. For example, the transition $1s(A_1) \rightarrow 4p_0$ for phosphorus, though obscured in the zero-stress spectrum in Fig. 1, manifests itself as a low-energy component for $\mathbf{F}||[100]$ and $\mathbf{E}||\mathbf{F}$. From the separation, α, of the low-energy components from the zero-stress positions of, say, $1s(A_1) \rightarrow 2p_0$ or $1s(A_1) \rightarrow 2p_\pm$ lines, one can deduce the zero-stress position of $1s(A_1) \rightarrow 4p_0$ line. This turns out to be 42.21 meV as compared to 42.25 meV from a direct observation in a suitable sample where conditions were optimum to resolve it.

Let us now consider the case of $\mathbf{F}||[110]$. The uniaxial stress for this case destroys all the threefold and the fourfold axes of symmetry; the two twofold axes [100] and [010] and the diagonal planes of reflection (101), (10$\bar{1}$), (011), and (01$\bar{1}$). The remaining elements of the point group T_d, viz., the planes of reflection (110) and ($\bar{1}$10) and the twofold axis of symmetry parallel to [001], define the new site symmetry C_{2v} which is a point group with orthorhombic symmetry. Table II shows again the steps leading to the determination of the irreducible representations of C_{2v} corresponding to each of the two components into which the excited states split. The selection rules for dipole transitions for this point group show they are polarized along [110], [1$\bar{1}$0], or [001] (see Fig. 8), depending on whether the excited state is characterized by the irreducible representations B_1, B_2, or A_1, respectively. We can now consider the polarization effects for different directions of the light propagation vector, $\mathbf{q}$ (see Fig. 8). In the first place it is obvious from Fig. 8 that the excitation spectrum should be the same for all $\mathbf{q}$ in the polarization $\mathbf{E}||\mathbf{F}$.

(*1*) $\mathbf{q}||[1\bar{1}0]$: for this direction of light propagation the transitions associated with the "B_2" representation will be absent for both $\mathbf{E}||\mathbf{F}$ and $\mathbf{E}\perp\mathbf{F}$. The allowed transitions for $\mathbf{E}||\mathbf{F}$ and $\mathbf{E}\perp\mathbf{F}$ are those shown in Fig. 9. Experiment shows that $1s(A_1) \rightarrow 2p_0(+)$ appears for

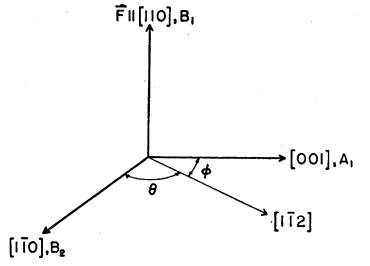

FIG. 8. The directions of polarization for electric dipole transitions with $\mathbf{F}||[110]$. For this orthorhombic point group C_{2v}, the orthorhombic axes are [110], [1$\bar{1}$0], [001]. The irreducible representation according to which the dipole moment along a given axis transforms is also shown.

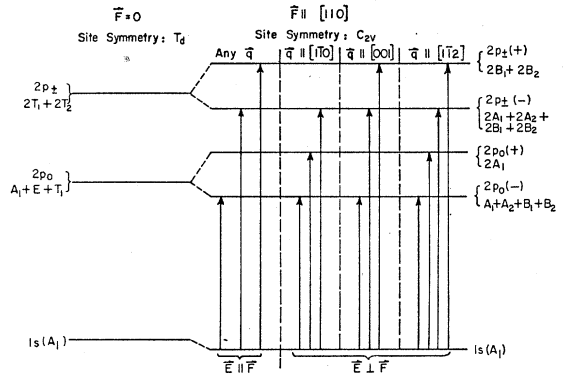

FIG. 9. Energy levels (not to scale) for $\mathbf{F}=0$ and $\mathbf{F}\|[110]$. The arrows indicate the allowed transitions for $\mathbf{q}\|[1\bar{1}0]$, $\mathbf{q}\|[001]$, and $\mathbf{q}\|[1\bar{1}2]$.

$\mathbf{E}\perp\mathbf{F}$ in agreement with the prediction. Also the transition $1s(A_1)\rightarrow 2p_0(-)$, though expected for both $\mathbf{E}\|\mathbf{F}$ and $\mathbf{E}\perp\mathbf{F}$, is observed for only $\mathbf{E}\|\mathbf{F}$. Thus, though allowed on the basis of the selection rules for $\mathbf{E}\perp\mathbf{F}$, the $1s(A_1)\rightarrow 2p_0(-)$ transition is evidently negligibly weak. This can be understood by an actual intensity calculation. Assuming effective mass wave functions for both $1s(A_1)$ and $2p_0(-)$, the calculations show that the transition is forbidden for $\mathbf{E}\perp\mathbf{F}$ and $\mathbf{q}\|[1\bar{1}0]$. The predictions for transitions to $2p_\pm(+)$ and $2p_\pm(-)$ are borne out by the experimental observations in that $1s(A_1)\rightarrow 2p_\pm(+)$ is observed for only $\mathbf{E}\|\mathbf{F}$ whereas $1s(A_1)\rightarrow 2p_\pm(-)$ can be seen for both $\mathbf{E}\|\mathbf{F}$ and $\mathbf{E}\perp\mathbf{F}$.

(2) $\mathbf{q}\|[001]$: For this direction of light propagation, the transitions associated with "A_1" representations are forbidden. The allowed transitions are indicated in Fig. 9. The most striking feature of this direction of propagation is the absence of the $1s(A_1)\rightarrow 2p_0(+)$ transition for both $\mathbf{E}\|\mathbf{F}$ and $\mathbf{E}\perp\mathbf{F}$, a feature predicted by theory and confirmed by observations. The transitions to $2p_\pm(+)$ and $2p_\pm(-)$ are expected for both $\mathbf{E}\|\mathbf{F}$ and $\mathbf{E}\perp\mathbf{F}$. This is in accordance with experimental observations.

(3) $\mathbf{q}\|[1\bar{1}2]$: This represents a case which is a superposition of the selection rules for both $\mathbf{q}\|[001]$ and $\mathbf{q}\|[1\bar{1}0]$ in that both "A_1" and "B_2" transitions are allowed. This is in agreement with experiments. The $1s(A_1)\rightarrow 2p_0(+)$ line should be observed for $\mathbf{E}\perp\mathbf{F}$. Its intensity compared to $\mathbf{q}\|[1\bar{1}0]$ should be reduced by $\cos^2\theta$, where θ is the angle between $[1\bar{1}0]$ and $[1\bar{1}2]$ directions. Experimentally the line is observed and the intensity is $\sim\frac{1}{3}$ that observed for $\mathbf{q}\|[1\bar{1}0]$. This is in good agreement with expectations. As discussed earlier, the $1s(A_1)\rightarrow 2p_0(-)$ transition though allowed for both $\mathbf{E}\|\mathbf{F}$ and $\mathbf{E}\perp\mathbf{F}$ for $\mathbf{q}\|[1\bar{1}0]$ is observed for only $\mathbf{E}\|\mathbf{F}$ showing that the transition associated with the A_1 representation is forbidden. For $\mathbf{q}\|[1\bar{1}2]$ the transition derives its intensity from the A_1 and B_2 representations for $\mathbf{E}\perp\mathbf{F}$. Thus in view of the results for $\mathbf{q}\|[1\bar{1}0]$, the intensity must be entirely due to the B_2 representation; and the ratio of intensities for $\mathbf{E}\perp\mathbf{F}$ for $1s(A_1)\rightarrow 2p_0(-)$ observed for $\mathbf{q}\|[1\bar{1}2]$ to that observed for $\mathbf{q}\|[001]$ should be $\cos^2\Phi=\frac{2}{3}$, where Φ is the angle between $[001]$ and $[1\bar{1}2]$ directions. Experimental observations are consistent with these predictions. Essentially, this orientation of $\mathbf{q}$ is an additional check on the observations for $\mathbf{q}\|[1\bar{1}0]$ and $\mathbf{q}\|[001]$.

A few general remarks may be made here regarding the other excited states. All the $m=0$ lines behave in an identical fashion with regard to their polarization. This is readily understood if one recognizes that all the corresponding lines labelled by $m=0$ are characterized by the same representations. Similar remarks apply to lines with $m=\pm 1$.

Let us finally consider the case for $\mathbf{F}\|[111]$. As we have already seen, no splittings are expected in this case. The new site symmetry is C_{3v} which is a uniaxial symmetry group, and polarization effects, i.e., dichroism may indeed have been expected in principle on this basis. As can be seen from Fig. 5, this is substantially the case. The $2p_0$ line appears to show an unresolved shoulder on the low-energy side and certain amount of dichroism seems to be present in all the lines. Further work is essential to derive significance from these features.

In conclusion, the splitting of the excitation lines of the substitutional group V donor and the pronounced polarization exhibited by the individual components can be understood by taking into account the shifts in energy of the conduction-band minima and the lowering of the donor symmetry. The excitation lines with $m=0$ all show a polarization pattern which is different from that for $m=\pm 1$, thus providing a technique for giving proper assignment to these levels. In this respect, stress effects are thus as useful as the Zeeman effect. From the identical splittings shown by all the lines, one can determine the deformation potential constant Ξ_u. The intensity of the components into which a given line splits under stress shows many interesting features which await further experimental work. The extension of the present technique to other types of donors should be of considerable interest.

ACKNOWLEDGMENTS

The authors wish to express their thanks to Professor P. Fisher and Professor S. Rodriguez for many useful discussions, and to Professor H. J. Yearian and Miss Louise Roth for orienting the crystals. Special thanks are due to R. L. Jones, who is responsible for the design of the strain jig used in the measurements.